Tellus (1988), *40A*, 285–302

Meridional heat transport by the atmosphere and the ocean: analysis of FGGE data

By KOOITI MASUDA, *Geophysical Institute, University of Tokyo, Yayoi, Bunkyo-ku, Tokyo 113, Japan*

(Manuscript received July 22, 1987; in final form January 7, 1988)

ABSTRACT

The annual mean meridional heat transport by the atmosphere is evaluated by using FGGE (First GARP Global Experiment) level IIIb data. The transport by the atmosphere-ocean system is estimated using satellite radiation observations from the Nimbus 7 ERB (Earth Radiation Budget) experiment. The annual mean transport by the ocean is obtained as the difference between the two values. The latitudinal distribution of transport by the total system exhibits good symmetry between the two hemispheres, with maximum poleward transport of 5.9×10^{15} W around 35° latitude N and S. Atmospheric and oceanic contributions to the transport exhibit large differences between the two hemispheres. In particular, in the subtropics of the northern hemisphere, the ocean carries more heat poleward than in the same latitude of the southern hemisphere. The poleward transport by the ocean at 20°–30°N evaluated in this study is about 3×10^{15} W, which is smaller by 0.5–1 $\times 10^{15}$ W than that found by Carissimo et al. but larger by 1–2 $\times 10^{15}$ W than recent estimates based on surface heat balance. The difference between the results of this study and Carissimo et al. comes from differences in estimates of the heat and moisture transport by mid-latitude atmospheric transient eddies.

1. Introduction

On an annual basis, the earth as a whole, including the atmosphere and the ocean, is approximately in a state of radiative energy balance. When we consider the meridional structure, the earth receives more energy than it emits in tropical latitudes, while the opposite is the case in polar latitudes. To attain a local balance, there must be transport of energy from the tropics to the polar latitudes, either by the atmosphere or by the ocean. The radiation budget of the earth can be observed from satellites. Estimates of the meridional energy transport differ from one another by as much as 1 PW (1 petawatt = 10^{15} watts) at 30°N where the transport takes a maximum value. (See, for example, Fig. 4 of Hastenrath 1982; more comparison will be given in Section 3).

The partition of the transport between the atmosphere and the ocean is harder to assess than the sum total. Various methods are reviewed by Bryan (1982). Direct evaluation of oceanic heat transport is possible through the use of hydrographic cross sections of temperature and salinity across ocean basins. However, it is difficult to yield meridional profiles of heat transport from currently available data. Oceanic and atmospheric modeling provides an opportunity to reveal the mechanisms of heat transport, but it cannot replace observational studies. One of the most successful methods, which can be traced back to Sverdrup (1957), has been the evaluation of oceanic heat transport from observed sea surface heat balance.

Another method was proposed by Vonder Haar and Oort (1973). It is to estimate the atmospheric transport from meteorological data and derive the oceanic transport by subtracting it from the radiation-based estimate of the total transport. These authors concluded that the contribution of the ocean to the heat transport is larger than many researchers had expected. According to Oort and Vonder Haar (1976), the ocean carries nearly 3 PW of heat polewards at 20°N. Recently, Carissimo et al. (1985) made a revised analysis with a similar technique and found that the oceanic transport at this latitude amounts to 3.5 PW. Since recent surface heat balance studies (Hsiung, 1985; Talley, 1984; Hastenrath, 1982) still give the value of 1 to 2 PW, the gap between the results of the two methods has become even larger. Sources of the discrepancy can be sought in the uncertainty of both methods. For the residual method in particular, the sparse data coverage in the tropics and in the southern hemisphere might lead to an under-estimated atmospheric transport and an over-estimated oceanic transport.

The First GARP Global Experiment (FGGE), also known as the Global Weather Experiment (GWE), which took place from 1 December 1978 through 30 November 1979, benefited from international cooperation in enhanced observation and compilation of reports. Gridpoint data sets called "FGGE level IIIb data sets" or briefly "FGGE IIIb data sets" are made from these observation reports at the European Centre for Medium-Range Weather Forecasts (ECMWF) and the Geophysical Fluid Dynamics Laboratory (GFDL). These are accomplished by "four-dimensional" assimilation systems which are integrated systems of interpolation and numerical forecast processes. In areas where no observations exist at a given time, forecast values are adopted. These have a physically realistic structure, though they depend on formulations of dynamical and physical processes of the model. It is expected that better coverage of observation along with the realistic patterns in poorly observed areas make the FGGE data superior to conventional station data analysis, even though a one-year period may be too short a sample of the present climate. In addition, the two centers used very different designs to assimilate the data; namely "intermittent assimilation" at ECMWF and "continuous assimilation" at GFDL (see, for example, Bourke et al., 1985). The difference between results from the two data sets can be a measure of possible errors of the current state of the art.

The observation of radiation budgets was also improved during this period. The equipment of the Earth Radiation Budget (ERB) experiment to measure the radiative fluxes of the whole spectral range started operation in October 1978 on the Nimbus 7 satellite (Jacobowitz et al., 1984b).

In this paper, heat transport by the atmosphere is evaluated by making use of FGGE IIIb data (Section 2). The heat transport by the ocean-atmosphere system is evaluated from radiative balance with the MATRIX data of Nimbus 7 ERB experiment (Section 3). The transport by the ocean is evaluated as the residual of the two, and is compared with the results of previous studies (Section 4). A brief conclusion is given in Section 5. Problems associated with FGGE IIIb data sets are discussed in a companion paper (Masuda, 1988).

2. Atmospheric energy transport derived from meteorological data

2.1. Method

2.1.1. Principle. In this study, the energy transport in the atmosphere is discussed in the form of energy quantities integrated vertically from the effective top of the atmosphere (p_{top}) to the earth's surface (p_s). The integration of an arbitrary quantity X,

$$\frac{1}{g}\int_{p_{top}}^{p_s} (X)\,dp = \int_{z(p_s)}^{z(p_{top})} (\rho X)\,dz \tag{1}$$

will be denoted with brackets as $\langle X \rangle$. When discussing the vertically integrated energy transport, it is convenient to introduce moist static energy (per unit mass) h as defined by the sum of enthalpy, potential energy and latent energy:

$$h = C_p T + gz + Lq. \tag{2}$$

The horizontal two-dimensional vector of the vertically integrated energy transport can be written as

$$\langle h v_H \rangle = \langle C_p T v_H \rangle + \langle gz v_H \rangle + \langle Lq v_H \rangle, \tag{3}$$

neglecting the minor contribution of kinetic energy transport. v_H is the two-dimensional vector of horizontal wind. The first term on the right-hand side of (3) is the sum of the advection of internal energy $\langle C_v T v_H \rangle$ and the "pressure term" $\langle p\alpha v_H \rangle = \langle RT v_H \rangle$. The divergence of the pressure term is equal to the vertically integrated work done by pressure, if we assume hydrostatic balance and vanishing exchange of mass at p_{top} and p_s (see Oort and Peixóto (1983)).

In this study, the meridional component of the energy transport vector, $\langle hv \rangle$, is calculated at each horizontal gridpoint, and integrated along each latitudinal circle. Thus the total transport across the latitude is

$$T_A = \int_0^{2\pi} a\cos\phi \langle hv \rangle \, d\lambda. \tag{4}$$

Actually, it is evaluated as the sum of three components, namely:

$$\begin{aligned} T_A = & \int_0^{2\pi} a\cos\phi \langle C_p(T - T_{gl})\, v \rangle \, d\lambda \\ & \qquad \text{(enthalpy transport)} \\ & + \int_0^{2\pi} a\cos\phi \langle g(z - z_{gl})\, v \rangle \, d\lambda \\ & \qquad \text{(potential energy transport)} \\ & + \int_0^{2\pi} a\cos\phi \langle Lqv \rangle \, d\lambda \\ & \qquad \text{(latent heat transport).} \end{aligned} \tag{5}$$

The quantity $C_pT + gz$ is the dry static energy, and the sum of the first two terms on the right-hand side is therefore the transport of dry static energy. To prevent loss of significant digits due to adding numbers of the same sign, two prescribed constants T_{gl} and z_{gl} are introduced. These represent approximate values of the global mean temperature and geopotential height, respectively. The expression (5) is arithmetically equivalent to (4) as long as no net exchange of mass occurs across a latitudinal circle, that is, when

$$\int_0^{2\pi} a\cos\phi \langle v \rangle \, d\lambda = 0 \tag{6}$$

holds. This condition is equivalent to that the divergence of the vertically integrated mass flux is zero,

$$\nabla_H \cdot \langle v_H \rangle = 0. \tag{7}$$

In reality, there is true mass flux divergence associated with the local change of surface pressure. However, it is generally smaller than the computed apparent mass flux divergence which has the order of magnitude of 10^{-3} kg m^{-2} s^{-1}. Thus, the assumption of vanishing mass flux divergence can be justified.

Though one of the aims of four-dimensional assimilation is to produce physically consistent fields of meteorological variables, actual products of assimilation do not perfectly satisfy the requirements. It is therefore necessary to adjust the wind field to ensure the above approximate condition of mass conservation. In the present study, the condition (7) is adopted in order to make a consistent estimate of energy flux divergence as well as energy transport. The vertical mean divergent wind is subtracted from the wind at each level to meet this condition. The vertical mean divergent wind is obtained by (a) vertically integrating wind components from p_{top} to p_s to give the total horizontal mass flux, (b) taking the divergence of the mass flux, (c) solving Poisson's equation on the sphere to give the potential function of mass flux, and (d) taking the gradient of the potential function and dividing it by the total mass of the air column. The procedure is basically the same as that adopted by Boer and Sargent (1985) and Boer (1986), except that a gridpoint method is used here instead of a spherical harmonic expansion for the solution of Poisson's equation. Because the poles are singularities of the latitude-longitude coordinate system, regular finite differences yield large errors in evaluating flux divergences. To cope with this, before applying the above procedure, the zonal and vertical mean is subtracted out from the meridional component of the wind in the row of gridpoints just next to the poles.

Making use of a time mean (denoted by an over-bar) and the deviation from it (a prime), the time mean transport of some quantity X can be decomposed into the transport by "stationary", $\overline{X}\,\overline{v}$, and "transient", $\overline{X'v'}$, motions:

$$\overline{Xv} = \overline{X}\,\overline{v} + \overline{X'v'}. \tag{8}$$

The zonal mean (denoted by square brackets) of the stationary part is further divided into the transport by the mean meridional circulation and by "stationary eddies" as:

$$[\overline{X}\overline{v}] = [\overline{X}]\,[\overline{v}] + [\overline{X}^*\overline{v}^*]. \tag{9}$$

where asterisks stand for deviations from the zonal mean. The term "the transport by transient eddies" is used as the synonym of the transport by transient motions, which is not decomposed into zonally symmetric and asymmetric parts.

In this study, time averages of three-month periods are considered. The periods, December-January-February (DJF), March-April-May (MAM), June-July-August (JJA) and September-October-November (SON), are referred to as "seasons" here without any implication for the question of the climatologically proper definition of seasons. The total transport during a season $\langle[\overline{Xv}]\rangle$ is calculated by a simple time average of twice-daily instantaneous transport values. The transport by time-mean motion $\langle[\bar{X}\bar{v}]\rangle$ is calculated from the seasonal mean field of meteorological variables. The transport by the mean meridional circulation $\langle[\bar{X}][\bar{v}]\rangle$ is evaluated by multiplying the mass-weighted zonal mean of the seasonal mean meridional wind $[\bar{v}]$ by that of the carried quantity $[\bar{X}]$. The transient eddy and stationary eddy transport are obtained from (8) and (9), respectively.

2.1.2. Processing of the ECMWF data. The first source of atmospheric data used in this study is the FGGE IIIb data set produced by ECMWF. This data set is called the "main IIIb" to distinguish it from the "final IIIb" (mentioned in Section 5). The data are given on a 1.875° longitude × 1.875° latitude (192 × 97) grid with 15 vertical levels in the pressure coordinate system, twice daily at 00 GMT and 12 GMT for the period from 1 December 1978 to 30 November 1979.

The primary analysis variables of the ECMWF assimilation system are the geopotential height (z), the horizontal wind components (u, v) at 15 standard levels, mean sea level pressure, and the specific humidity integrated with respect to pressure within each interval between standard levels below 300 hPa (5 layers). The officially published ECMWF FGGE IIIb data set contains temperature and relative humidity at standard levels (instead of layer-integrated specific humidity). Those quantities were computed from the primary analysis variables using their normal mode initialization routine. The data set is described by Bengtsson (1983) and Bengtsson et al. (1982). The scheme of the interpolation process is more thoroughly explained by Lorenc (1981) for mass and wind, and by Lorenc and Tibaldi (1980) for moisture.

In the present study, the 50 hPa level is assigned as the upper boundary, p_{top}. The data quality above this level is generally not good because observations were few. The data at the 15hPa level of the ECMWF data set are also excluded because they suffer from the inadequate partition of the 100–200 hPa thickness from satellite observations during the first half of the FGGE period (Julian, 1983; Lambert, 1983). (The omission of the 150 hPa level might introduce another kind of bias into the analysis in this study.)

The lower boundary p_s is the surface pressure. The height of the orographic surface of the 1.875° gridpoint model used during the "main" IIIb assimilation at ECMWF (called "the old orography" by Kållberg and Uppala, 1985) is adopted. The pressure is interpolated to the bottom surface by referring to the geopotential height at standard levels at each assimilation time. It is assumed here that the difference of the height is proportional to the difference of the logarithm of the pressure.

Constant values of C_p (specific heat of air at constant pressure) $= \frac{7}{2} R$, R (gas constant for air) $= 287.05$ J K^{-1} kg^{-1} and L (latent heat of vaporization of water per unit mass of water) $= 2.50 \times 10^6$ J kg^{-1} are used.

The atmosphere is divided into 10 layers according to the 11 standard levels where the data values are available. The configuration of the layers in this study is shown in Fig. 1a. To define a proper lower boundary condition, the layer which contains the ground surface is modified to have the bottom at the ground. In places where $p_s > 1000$ hPa, the lowest layer is extended to the ground. In layers completely below the orographic surface, as marked "o" in Fig. 1, zero transport is assigned. When applied to the computation of divergences of energy and moisture fluxes (which will be published in other papers), this procedure yields better (though not very satisfactory) results in mountainous areas such as the Tibetan Plateau, than the usual finite differences on standard pressure levels.

Every variable is converted into a layer-mean or layer-integrated quantity. The geopotential height z and the horizontal wind components (u, v) are linearly interpolated in pressure to the middle of each layer (denoted by dash-dotted lines in Fig. 1). The temperature T is calculated from the geopotential height with the corrections for the buoyancy of water vapor as suggested by Bengtsson (1983). The calculation of the moisture transport is made only for layers below 300 hPa. The omission of moisture in the upper layers does not substantially affect the vertically integrated transport, because the absolute humidity in the upper layers is quite small. To obtain layer-mean

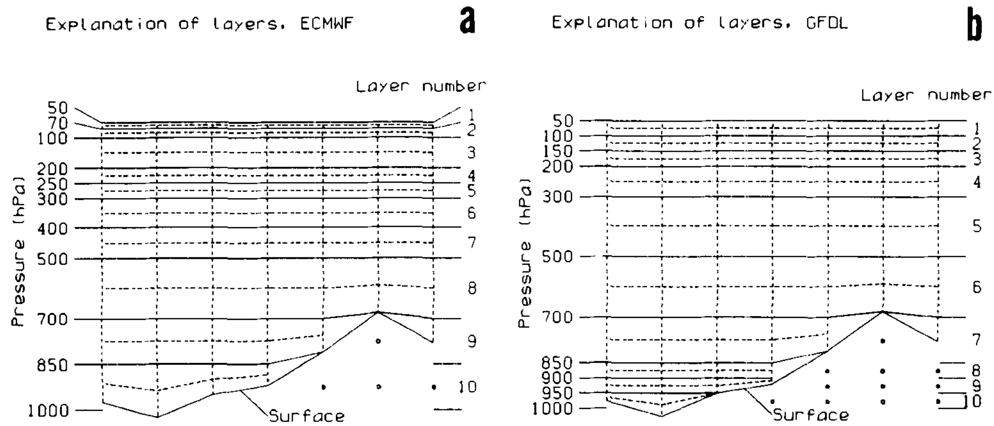

Fig. 1. Explanation of layers adopted in this study for the analysis of (a) ECMWF and (b) GFDL data. The dash-dotted lines indicate the middle level of each layer. The marks "o" indicate those levels which are completely underground.

specific humidity, relative humidity and temperature of the IIIb data set are first interpolated to the middle of each layer, and then converted to specific humidity at this level. The result is compared with the original layer-integrated moisture content data, which were made available by courtesy of Dr. M. Kanamitsu for part of the FGGE year (Masuda, 1988). Though a somewhat different method is applied for the reproduction from relative humidity there, the method of the present study yields similar results. In general, the moisture content in the layers 6, 7, 8, and 9 (see Fig. 1(a)) is successfully reproduced. That of the lowest layer is, however, 10% smaller than the original layer-integrated value. This discrepancy seems to be due to the extrapolation scheme used at ECMWF to produce standard level values from layer values. To compensate for this bias, the moisture content of the layer 10 of the ECMWF data set is multiplied by a factor of 1.11.

2.1.3. Processing of the GFDL data. The second source of atmospheric data is the FGGE IIIb data set produced by GFDL, which is described by Miyakoda et al. (1983). This is also called the "main IIIb" data set. The assimilation scheme is explained by Stern et al. (1985). In this study, the monthly statistics tape provided by courtesy of Dr. N.-C. Lau of GFDL is used. Some of the statistics are presented graphically in the reports by Lau (1984a,b, 1985). The data set contains monthly mean values and covariances, calculated from twice-daily values, of geopotential height, temperature, specific humidity, and horizontal and vertical wind components. The resolution of data is 3.75° longitude × 1.875° latitude with 12 levels ranging from 10 hPa to 1000 hPa (extracted from 1.875° longitude × 1.875° latitude and 19 levels of the official IIIb data).

The processing of GFDL data in this study is the same as the ECMWF data except for the following points. (1) The fluxes by transient eddies with periods shorter than a month are added to the fluxes for monthly mean fields in order to account for all of the atmospheric transport resolvable by twice-daily time intervals. (2) The configuration of layers is shown in Fig. 1(b). The surface pressure p_s is calculated by interpolating pressure at the orographic height of the rhomboidal-30 spectral model used for the assimilation, referring to the monthly mean standard level geopotential height. (3) The temperature and the specific humidity from the statistic tape is used directly. (4) All meteorological variables are interpolated linearly in p to the middle of each layer. This procedure may over-estimate the specific humidity. However, the degree of over-estimation is small in this case, because the pressure intervals in the lower troposphere are small. (5) Moisture transport is evaluated at all layers.

2.1.4. Processing of Oort's statistics. It is interesting to compare the results of the FGGE analyses with the comprehensive statistics of the global atmospheric variables compiled by Oort (1983). This is the same data set as was used by Carissimo et al. (1985). The statistics are based on radiosonde station data and surface ship data of the ten-year period from May 1963 to April 1973. Monthly means and covariances at each station were first calculated and converted to $5^\circ \times 5^\circ$ gridpoint data by a relaxation method. For gridpoints where there are no stations nearby, covariance values relaxed from surrounding gridpoints were given. To obtain the mean meridional circulation, Oort used indirect evaluation from the balance of angular momentum for latitudes poleward of 20°, direct averaging for latitudes equatorward of 10°, and interpolation of the two results in between. The transport of heat and moisture in the atmosphere was discussed by Oort and Peixóto (1983) and Peixóto and Oort (1983).

In the present study, 10-year composites of seasonal (3-month) means and covariances of Oort (1983) are used. The "vertical mean" of zonally averaged meriodional fluxes of temperature, of geopotential height and of specific humidity are taken from the microfiches attached to the publication of Oort (1983). These are multiplied by the annual mean atmospheric mass over each latitudinal circle which is tabulated in his Table 14.

2.2 Results

2.2.1. Mass conservation. Before proceeding to the energy transport, let us examine the apparent mass transport, since the error in the mass budget can cause a proportional error in the energy budget. When the original gridpoint data contain some erroneous component of the mass transport, there is some arbitrariness in how to distribute the correction. In this study, a correction independent of altitude is adopted (as noted in subsection 2.1.1). Other choices would lead to somewhat different values of the energy transport.

The annual mean and vertically integrated apparent meridional transport of mass is shown in Fig. 2. Results from both data sets have a peak in the northward transport near the equator. The magnitude is about 4 times larger in the GFDL analysis. Considering that the typical range of

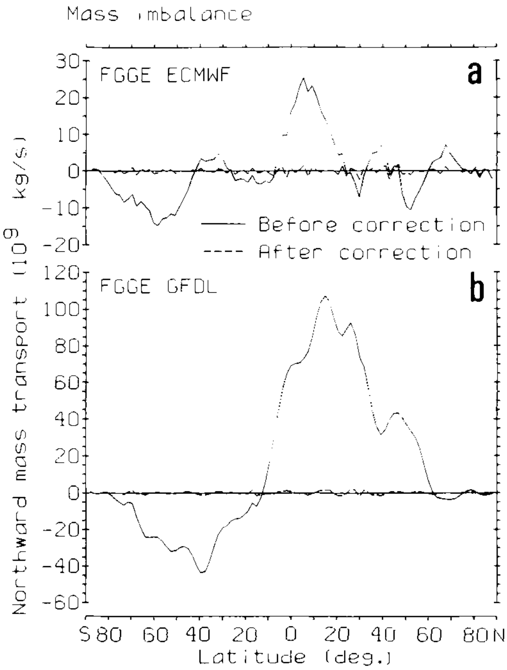

Fig. 2. Annual mean northward apparent mass transport resulted from the analyses of (a) ECMWF and (b) GFDL data. The solid line denotes the transport as directly obtained from the data; the dashed line denotes the transport after the correction applied in this study.

moist static energy in the average vertical profile of the troposphere in the equatorial region is about $2\text{–}3 \times 10^4$ J kg^{-1}, the apparent mass transport of 2.5×10^{10} kg s^{-1} in the ECMWF data set corresponds to the uncertainty of the energy transport of 0.5–0.75 PW. Similarly, the uncertainty of the GFDL analysis due to the inconsistency of mass is 2–3 PW.

The divergence of the apparent mass flux is also calculated (Masuda, 1988). Large absolute values of flux divergence are found over large mountains. Thus, it is suspected that the main source of the inconsistency in mass is the vertical interpolation between the pressure coordinate and terrain-following "sigma" coordinate. At GFDL, the interpolation process is performed on the sigma levels, where mass balance is satisfied (Miyakoda, personal communication). The resultant field is interpolated to standard pressure levels for the official archives. At the same time, the field is horizontally interpolated from Gaussian latitudes of approximately 2.2° interval to equally-spaced latitudes of 1.875° interval. These procedures of interpolation are the source of inconsistency. At ECMWF, the interpolation step of four-dimensional assimilation is performed on levels of the pressure co-ordinate, where there is no guarantee of mass conservation. The forecast field used as the initial guess is consistent on the sigma levels but must be interpolated to the pressure levels. The larger inconsistency of mass in GFDL data compared with ECMWF data seems to be due to the larger activity of external gravity waves apparent in the surface pressure field (Puri and Stern, 1985).

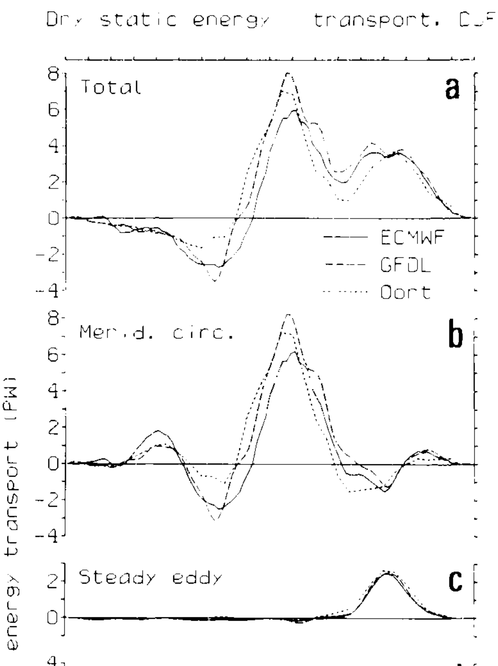

Fig. 3. Northward transport of dry static energy during DJF (December-January-February) in PW. (a) Total transport; (b) transport by the mean meridional circulation; (c) transport by stationary eddies; (d) Transport by transient eddies. For all panels, the solid lines show the results obtained from ECMWF data, the dashed lines from GFDL data, and the dotted lines from Oort's (1983) statistics.

2.2.2. Transport of dry static energy. The transport of dry static energy (the sum of the transport of enthalpy and potential energy) in the atmosphere during DJF and JJA is shown in Figs. 3 and 4, respectively. The total transport (panel a) can be decomposed into the transport by the mean meridional circulation (b), stationary eddies (c) and transients (d). The results from the FGGE analyses confirm the following qualitative features previously noted by, for example, Oort and Peixóto (1983): the mean meridional circulation is dominant in the tropics; transients (mainly extratropical cyclones) are most important in the mid-latitudes; stationary eddies (mainly planetary waves) are also important in the northern-mid latitudes in winter. The transport by the transients in the northern mid-latitudes in summer (Fig. 4d) is smaller than that in the southern

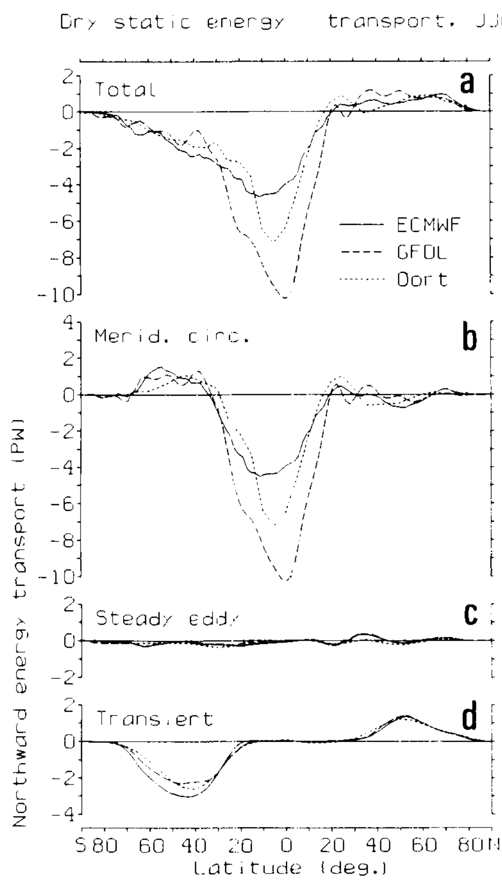

Fig. 4. Northward transport of dry static energy during JJA (June-July-August). For explanation, see Fig. 3.

mid-latitudes in summer (Fig. 3d). The transport of gz by transient eddies is negligible, as is anticipated from the fact that it is exactly zero in the geostrophic case, so that the transient transport of dry static energy is essentially that of C_pT.

The transport of dry static energy by the mean meridional circulation is the residual of two opposing components: namely the transport of air with larger C_pT in the lower branch and an opposite transport of air with larger gz in the upper branch. Fig. 5 shows the transport of enthalpy and potential energy by the mean meridional circulation, and Fig. 6 shows the field of zonal mean meridional wind. Both figures are for the JJA season. We recognize two Hadley (direct) cells in the tropics and two Ferrel (indirect) cells in the mid-latitudes. Lower level convergence and upper level divergence are dominant at the intertropical convergence zone (ITCZ) of the summer hemisphere. In other words, the Hadley cell of the winter hemisphere is strengthened and extends beyond the equator.

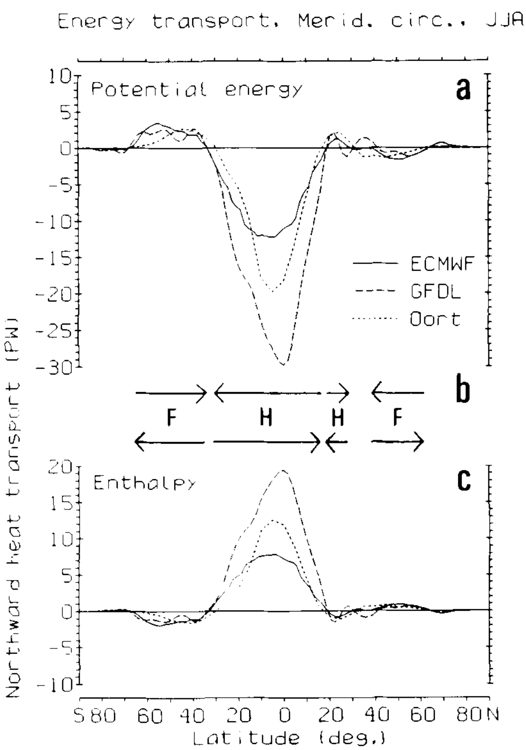

Fig. 5. Northward transport of (a) potential energy gz and (c) enthalpy C_pT by the mean meridional circulation during JJA. The lines are as explained in Fig. 3. In panel (b), letters "H" and "F" denote Hadley cells and Ferrel cells, respectively, and the arrows show the direction of mean meridional wind in the upper and lower branches of the cells.

The GFDL data show a stronger Hadley circulation than the ECMWF data in spite of the fact that the observations used for the assimilation were basically the same. In particular, the cross-equatorial flow during JJA observed with the GFDL data is twice as strong as that observed with the ECMWF data. The same is valid for the northward transport of C_pT and the southward transport of gz. A similar feature was demonstrated by Kung and Tanaka (1983) and Lau (1984b) for May and June of 1979. The disagreement of two datasets is related to the difference in amplitude of the divergent motion in the tropics. It is suspected that the ECMWF assimilation scheme tends to suppress the divergent motion, while the GFDL scheme tends to emphasize it (Julian, 1985). In the ECMWF scheme, at least two factors are likely to contribute to underestimating the divergence. First, in the interpolation process, the covariance matrices of the observational errors were formulated with the assumption of no divergence. They essentially filtered out the divergent component of the observed wind field (Ikawa, 1984; Daley, 1985). Second, in the normal mode initialization process, adiabatic motion was assumed. This resulted in a severe suppression of gravity-wave modes, which contain most of the divergence. In the GFDL scheme, wind and height observations were interpolated separately. In addition, GFDL had difficulty in separating out erroneous observational reports. Thus, gravity waves were easily excited by the imbalance of wind and height fields. In view of the above, it may be surmised that the true magnitude of the Hadley circulation is somewhere between the two analyses, presumably close to Oort's analysis. Since the two components C_pT and gz are contributing in opposite directions, the effect of the uncertainty in the total energy transport is smaller than that of each component. In addition, the errors in the two extreme seasons (JJA and DJF) tend to cancel each other.

In the middle latitudes of the northern hemisphere, we find a good agreement between ECMWF and GFDL for the transport by

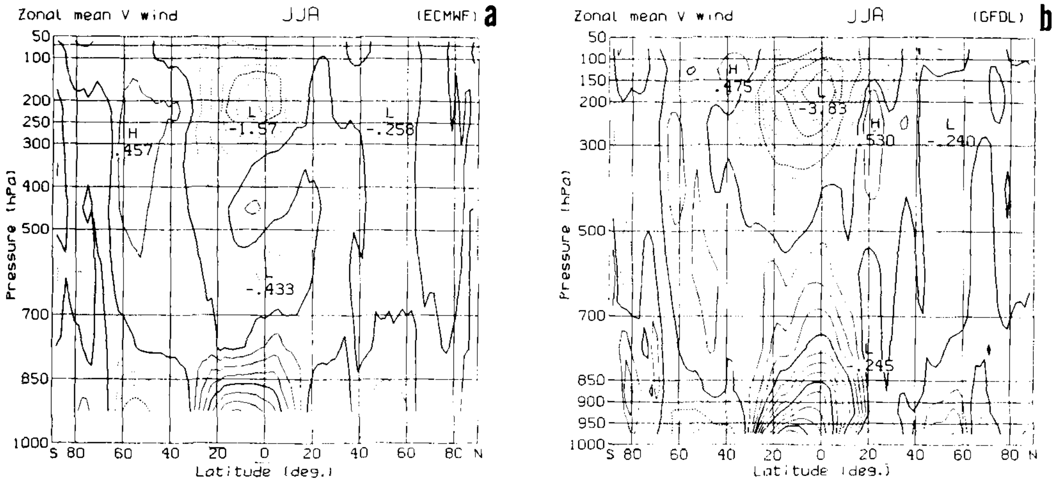

Fig. 6. Meridional-vertical plot of zonal mean meridional wind during JJA of (a) ECMWF and (b) GFDL data. The units are (m s^{-1}). The interval between thick contour lines is 1 m s^{-1} and between thin contour lines 0.25 m s^{-1}. Dashed lines indicate negative values (northerlies).

transients. Both datasets give about 1 PW larger transport than Oort's analysis does in winter (DJF) as well as in spring and autumn. Since extratropical cyclones often intensify over the ocean where there are few conventional upper-air observations, it is likely that Oort's analysis under-estimates the transport by transients.

In the southern hemisphere mid-latitudes, the ECMWF data give a larger poleward transport by transients than do the GFDL data. It was learned from drifting buoy observations during FGGE that the surface pressure in the extratropical cyclones in the southern ocean was deeper than what had been expected (Guymer and Le Marshall, 1980). The ECMWF assimilation scheme accommodated those buoy observations while the GFDL scheme often rejected them. This fact was considered a weakness of the GFDL scheme, so attempts to improve acceptance have been made after the "main" IIIb assimilation (Stern et al., 1985; Puri and Stern, 1985). In this context, the result from the ECMWF data seems to be more faithful to reality of the FGGE year. Meanwhile, Trenberth (1984) claimed that the FGGE year is not a good example of climatology, because the surface pressure around 60°S was extraordinarily low during that year. Since we do not have data of other years with as good quality as the FGGE IIIb data, we cannot quantitatively answer the question of how anomalous the energy transport was during the FGGE year.

2.2.3. Transport of moisture. The transport of latent energy, that is, the transport of moisture multiplied by the latent heat of evaporation per unit mass of water is shown in Figs. 7, and 8 for DJF and JJA, respectively. In the tropics, moisture is transported by the lower branch of the Hadley cells. Together with C_pT, it nearly compensates for the transport of gz by the upper branch. We again see the difference among the three analyses concerning the Hadley circulation. Besides being carried by the meridional circulation, moisture is carried by transient motion down-gradient from the equatorial region to the subtropics. In middle latitudes, moisture is carried mainly by transient eddies. The differences observed among the various analyses are similar to those seen in the dry static energy transport.

Around 20° N in JJA, the FGGE analyses yield a 1.5–2 PW northward transport of latent energy. The contribution of stationary eddies more than compensates for the southward transport by the nothern (minor) Hadley cell. Oort's analysis gives the value of 0.5 PW. A breakdown into the three

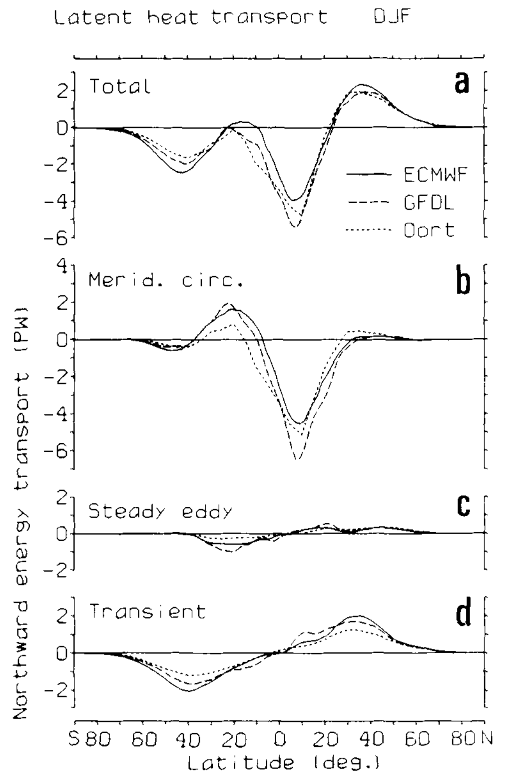

Fig. 7. Northward transport of latent energy during DJF (December-January-February). For explanation , see Fig. 3.

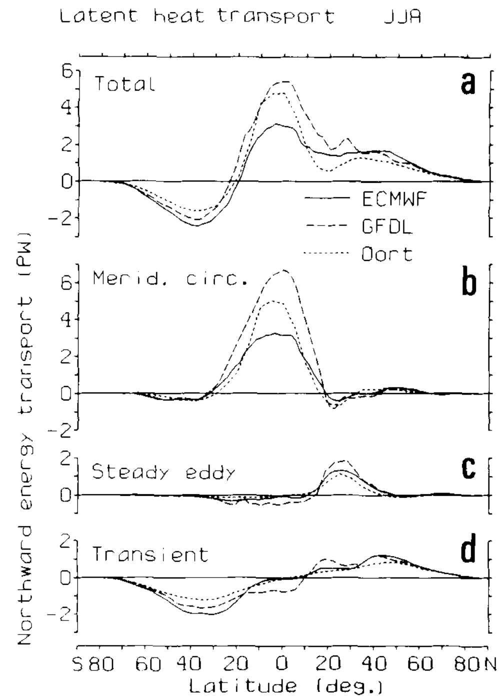

Fig. 8. Northward transport of latent energy during JJA (June-July-August). For explanation, see Fig. 3.

components shows that all three contribute to the difference between FGGE analyses and Oort's analyses. Examination of the geographic distribution of moisture fluxes (figure omitted) reveals that Oort's analysis (Fig. 8 of Peixóto and Oort, 1983) did not capture the moisture transport by the monsoon circulation over the Arabian Sea.

2.2.4. Transport of moist static energy. The mean transport of moist static energy during the four seasons is shown in Fig. 9. The transport in mid-latitudes is larger in winter than in summer in both hemispheres. But the magnitude of seasonal change is different. The transport in the northern hemisphere in summer (JJA) is less than one half of the that in winter (DJF), and the transport in spring and autumn is also considerably smaller than in winter. On the other hand, the transport in the southern hemisphere in summer (DJF) is about $\frac{3}{4}$ of that in winter, and the transport in spring and autumn is nearly the same as that in winter.

The transport across the equator is small according to the ECMWF data. The smallness is reasonable, considering that the mean meridional circulation is the dominant energy transporter and that the moist static energy near the tropopause is approximately equal to that near the surface in the equatorial area. The GFDL data show net southward transport by 4 PW during the JJA season.

The annual mean transport is shown in Fig. 10. The agreement between the two FGGE data sets is good north of 30°N. The peak value of the northward transport is about 4 PW at 40°N. The value is 1 PW larger than the value obtained from the statistics of Oort (1983). There is a large difference between the two FGGE data sets concerning the transport across the equator: according to the GFDL data, large southward transport during the JJA season is not compensated for in other seasons. There is also a

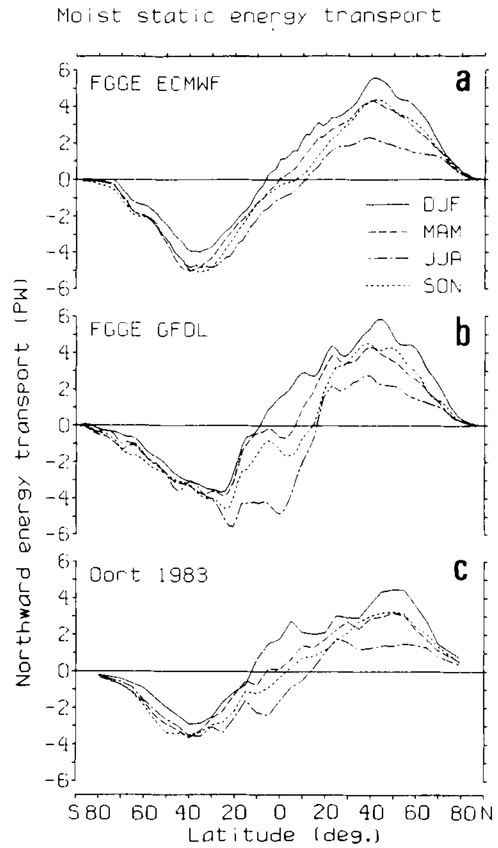

Fig. 9. Northward transport of moist static energy during the four seasons from the analyses of (a) ECMWF, (b) GFDL and (c) Oort (1983). The solid lines are for DJF, dashed lines for MAM, dash-dotted lines for JJA, and dotted lines for SON seasons.

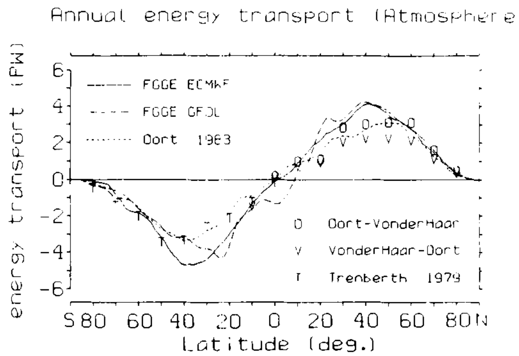

Fig. 10. Annual mean northward transport of moist static energy. The solid lines show results obtained from FGGE ECMWF data, dashed lines from FGGE GFDL data, and dotted lines based on Oort's (1983) statistics. Symbols "O" stands for Oort and Vonder Haar (1976), "V" for Vonder Haar and Oort (1973), and "T" for Trenberth (1979).

difference in the southern mid-latitudes. The peak value of southward transport is 4.7 PW at 40°S in the ECMWF analysis, while it is 4.2 PW at 20°S in the GFDL analysis.

The partition of the annual mean transport between the transport of dry static energy and that of latent energy is shown in Fig. 11. Overall, the two components have a similar order of magnitude. The transport of dry static energy is poleward in most latitudes, while the transport of moisture is equatorward in the tropics. The difference in moisture transport values between the two FGGE analyses is small, despite many uncertainties in both data sets.

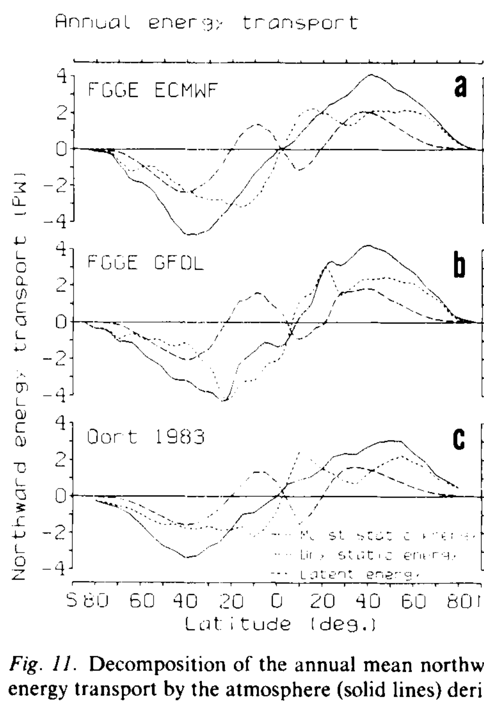

Fig. 11. Decomposition of the annual mean northward energy transport by the atmosphere (solid lines) derived from (a) ECMWF, (b) GFDL and (c) Oort's data into the contributions of dry static energy (dotted lines) and latent energy (dashed lines).

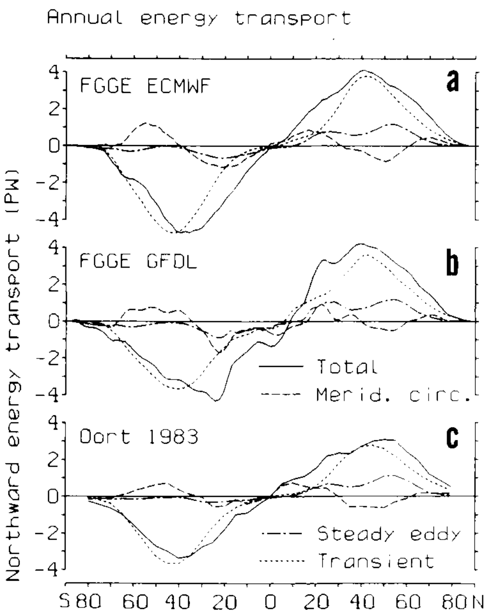

Fig. 12. Decomposition of the annual mean northward moist static energy transport (solid lines) derived from (a) ECMWF, (b) GFDL and (c) Oort's data into the contributions of the mean meridional circulation (dashed lines), stationary eddies (dash-dotted lines) and transient eddies (dotted lines).

The decomposition of energy transport into the transport by mean meridional circulation, by stationary eddies and by transient motions is shown in Fig. 12. Here, the decomposition is based on seasonal averages, not on annual ones as was done by Oort and Peixóto (1983). Again we confirm that the dominant component is the mean meridional circulation in the tropics and transients in the mid-latitudes. In addition, stationary eddies play an important role in the nothern mid- to high latitudes in winter (planetary waves) and in the northern subtropics in summer (monsoon).

3. Transport by the atmosphere-ocean system derived from satellite radiation data

3.1. Principle

If interannual variations of energy storage can be ignored, the total amount of energy that must be transported in a year by the atmosphere or by the ocean can be deduced from the net radiation budget (Vonder Haar and Oort, 1973). When a latitude belt has net income F_{net} in the radiation budget, the belt must lose energy through meridional transport in the atmosphere T_{A} or in the ocean T_{O}. Thus,

$$a \cos\phi \, F_{\mathrm{net}} + \frac{1}{a} \frac{\mathrm{d}}{\mathrm{d}\varphi} (T_{\mathrm{A}} + T_{\mathrm{O}}) = 0. \qquad (10)$$

Therefore, $T_{\mathrm{A}} + T_{\mathrm{O}}$ can be evaluated by integrating the net radiation with respect to latitude ϕ:

$$T_{\mathrm{A}}(\phi) + T_{\mathrm{O}}(\phi) = -\int_{\pi/2}^{\varphi} a^2 \cos\phi' \, F_{\mathrm{net}}(\phi') \, \mathrm{d}\phi', \qquad (11)$$

or in discrete form,

$$T_{\mathrm{A}}(\phi_k) + T_{\mathrm{O}}(\phi_k) = -\sum_{j=1}^{k} a^2 (\sin\phi_j - \sin\phi_{j-1}) \, F_{\mathrm{net}}(\phi_{j-\frac{1}{2}}) \, \Delta\phi. \qquad (12)$$

3.2. Processing of Nimbus 7 ERB data

In this study, monthly mean values in the MATRIX tapes of Nimbus 7 Earth Radiation Budget (ERB) experiment (Jacobowitz et al., 1984a,b) during the FGGE period are used. The Nimbus 7 ERB equipment has both narrow field of view (NFOV) scanning sensors and wide field of view (WFOV) non-scanning sensors. MATRIX tapes contain the net radiation values from each set of sensors in a quasi-equal-area grid, which has a 4.5° latitudinal width and approximately 600 km east-west extent.

Data from both sets of sensors are used to evaluate the annual mean transport. No WFOV data are given for latitudes higher than 81° because the orbit of the satellite does not pass these latitudes. The values for the adjacent latitude belt (76.5°–81° in each hemisphere) are assumed to be valid for the polar regions. Many NFOV observations are missing for the northern winter of 1978/79 due to the special operation of LIMS (Limb Infrared Monitor of the Stratosphere) equipment (Jacobowitz et al., 1984a). With a scatter diagram of all available monthly grid values of NFOV and WFOV data, it is found that the two sets of data are almost linearly correlated with a slope of unity and a bias of 13.0 W m^{-2} (WFOV is larger), where the correlation coefficient is 0.986. Therefore, WFOV values are substituted with the correction of the mean bias where the NFOV values are missing. The balance over the whole globe is -3.16 W m^{-2} for the NFOV data and $+9.58$ W m^{-2} for the WFOV data. The minor difference between these values and those tabulated by Jacobowitz et al. (1984a) is due to the somewhat different time periods and the different ways for filling missing data. Though the examinations of ERB observations (e.g., Arking and Vemury, 1984) suggest that the bias between the WFOV and NFOV observations comes from calibration problems in both sets of sensors, it is difficult for users of processed MATRIX data to make detailed corrections. Consequently, a simple scheme is adopted in this study, namely, the global mean value is subtracted out from all grid values of net radiation before the integration of expression (12). Without the correction, the transport at the end of the pole-to-pole integration would be -1.6 PW for the NFOV data and $+4.9$ PW for the WFOV data. A similar cumulative error from the radiation budget of Campbell and Vonder Haar (1980) would be $+5.1$ PW according to Oort and Peixóto (1983) and about $+4.3$ PW according to Carissimo et al. (1985).

Observations taken by the two sets of sensors have a different nature. While the NFOV sensors observe the radiation from target areas of approximately (150 km)^2 along several scanning planes around the sub-satellite point, the WFOV sensors are designed to observe radiation from the total area of the earth visible from the satellite. The WFOV system has an advantage in evaluating the total radiative flux from the earth, including the emission in oblique directions. However, some deconvolution process would be necessary to evaluate the spatial derivative of the net radiation over the globe from the WFOV data. On the other hand, the simple finite difference formula (12) is adequate for the NFOV data. Therefore, the results from the NFOV data are selected for this study. Another advantage of the NFOV data is that the magnitude of the global mean residual is smaller.

3.3 Results

Fig. 13 shows the annual mean northward energy transport. A similar result was obtained by Hartmann et al. (1986), with the same data set. The values adopted in previous transport studies are also shown. The NFOV curve shows

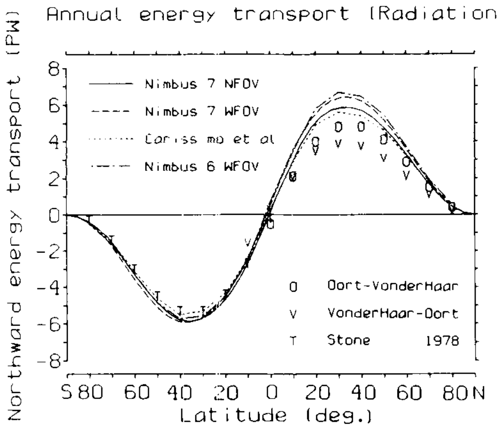

Fig. 13. The annual mean northward energy transport by the atmosphere-ocean system inferred from radiation observations. Solid lines show the results from Nimbus 7 NFOV data, dashed lines from Nimbus 7 WFOV data, dotted lines from Carissimo et al. (1985), and dash-dotted lines from Nimbus 6 WFOV data (Hastenrath, 1982). Symbols "O" stands for Oort and Vonder Haar (1976); "V" for Vonder Haar and Oort (1973); and "T" for Stone (1978), adopted by Trenberth (1979).

good symmetry about the equator. The peaks are found around 35° latitudes in both hemispheres, where the value is 5.9 PW.

The discrepancy among the curves is largest at 20–40° N. The difference between the NFOV curve and that of Carissimo et al. is small. The WFOV curve is about 1 PW higher than the NFOV curve. The curve based on Nimbus 6 ERB WFOV observations during 1975–1976 (quoted from Fig. 2 of Hastenrath, 1982) appears even higher at these latitudes. The systematic difference between WFOV and NFOV may be due to the difficulty in interpreting the WFOV data mentioned above. Alternatively, it may be due to the fact that WFOV observations cannot capture the minimum of outgoing infrared radiation associated with large amounts of upper clouds at the narrow ITCZ over the oceans. Vonder Haar and Oort (1973), Oort and Vonder Haar (1976) and some other older studies give values 1–2 PW lower than recent ones at these latitudes, while Newton (1972) gives values (not reproduced here) close to the recent ones. Interestingly, the difference among the analyses are quite small for the southern hemisphere.

4. Oceanic energy transport

The annual mean energy transport by the ocean is estimated by subtracting the atmospheric transport obtained in Section 2 from the total transport given in Section 3. The result is shown in Fig. 14 together with those of earlier studies. The evaluation of seasonal oceanic transport requires the evaluation of the surface heat exchange and oceanic heat storage, which are beyond the scope of this study.

The solid line in Fig. 14a is the estimate derived from ECMWF FGGE data and Nimbus 7 NFOV data. The pattern of oceanic transport is very different between the two hemispheres. In the northern hemisphere, a peak of northward transport appears around 25° N, where the value is about 3 PW. In the southern hemisphere, there are two peaks at 50°S and 20°S, where the values are less than 2 PW. The main reason for the difference between the two hemispheres is due to the difference of atmospheric transient eddy activity in summer, spring and autumn mentioned in subsection 2.2.4. The oceanic transport at 70°S is 0.6 PW, which should be nearly zero in reality because there is a negligible area of ocean at that latitude.

The GFDL analysis (dashed line) gives a northward transport of 4 PW around the equator and a southward transport somewhat larger than the ECMWF analysis does around 50°S. Both features do not seem to be reliable since they are related to problems of the GFDL data.

The poleward transport around 25° N and 25°S in both FGGE analyses is about 1 PW smaller than the result of Carissimo et al. (1985), reflecting a larger atmospheric transport. The agreement with Oort and Vonder Haar (1976) is fortuitous, since both the total transport and the atmospheric transport are 1 PW larger than their results.

The values from surface heat budget studies are shown in Fig. 14, panel (b). Roughly speaking, the resultant curves of those studies are similar. However, some biases exist among them, indicating that the heat budget over polar oceans is the most uncertain.

The agreement between results of FGGE analyses and surface heat budgets is good over the southern subtropics. They also agree with the combined direct estimate from hydrographical

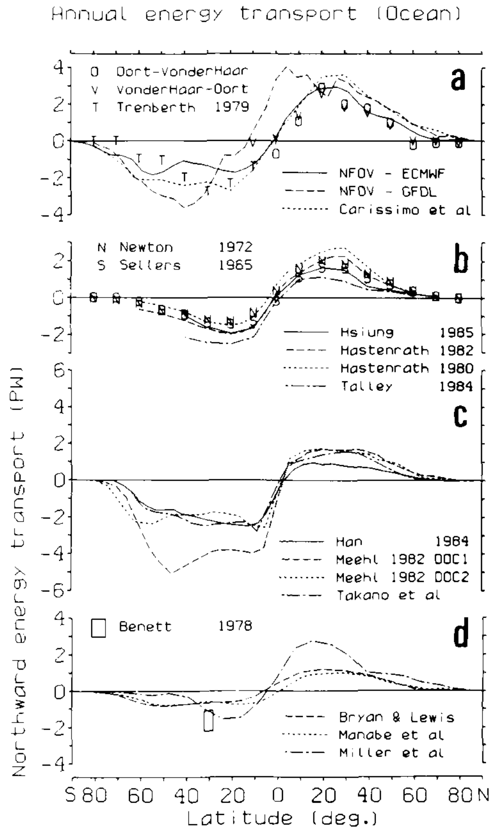

Fig. 14. The annual mean energy northward transport by the ocean. Panel (a): *those evaluated by the residual method.* The solid line shows the results from Nimbus 7 NFOV and FGGE ECMWF data; the dashed line, Nimbus 7 NFOV and FGGE GFDL data, the dotted line, Carissimo et al. (1985). The symbols "O" stands for Oort and Vonder Haar (1976); "V", Vonder Haar and Oort (1973); "T", Trenberth (1979). Panel (b): *those evaluated by the surface heat budget method.* The solid line, Hsiung (1985); the dashed line, Hastenrath (1982); the dotted line, Hastenrath (1980); the dash-dotted line, Talley (1984); "N", Newton (1972); "S", Sellers (1965). Panel (c): *those evaluated by ocean models.* The solid line, Han (1984); the dashed line, experiment DOC1 of Meehl et al. (1982); the dotted line, experiment DOC2 of Meehl et al. (1982); and the dash-dotted line, Takano et al. (unpublished, 1973) as displayed by Takano (1979). Panel (d): *those evaluated by various methods.* The dashed line, ocean model of Bryan and Lewis (1979); the dotted line, coupled ocean-atmosphere model by Manabe et al. (1979), the dash-dotted line, atmospheric model by Miller et al. (1983). The box drawn with solid line indicates the hydrographical estimate by Bennett (1978).

sections by Bennett (1978) who concluded that the southward transport across 28°–32°S is 1.15–2.27 PW (this is indicated by a rectangle in Fig. 14d). In the northern subtropics, on the other hand, the FGGE analyses indicate a poleward transport larger by 1 to 2 PW. This disagreement is difficult to explain. A weak point in the evaluation of the surface flux is the net radiative flux. Most of the investigators use empirical formulae involving surface temperature, humidity and cloudiness, similar to those proposed by Berliand and Berliand (see Budyko, 1971, ch. 2). Since there are very few stations that observe radiation over and around tropical oceans, the calibration of the coefficients for the empirical formulae may be inadequate. On the other hand, it is possible that the resolution of currently available atmospheric data is insufficient. In case of the ECMWF data, for example, the resolution is limited by their 660 km "analysis boxes" (see Lorenc, 1981) and the intervals between standard pressure levels. Those kinds of atmospheric circulation which have smaller scales than resolvable may contribute to heat and moisture transport: cold surges, intense tropical storms, or sub-synoptic scale cyclones along subtropical fronts such as the Baiu (Mei-yu) front over East Asia, to name a few.

Large differences are found among the results of oceanic models (Fig. 14, panel (c) and part of panel (d)). These reflect uncertainty of effective diffusion and viscosity in models which cannot resolve mesoscale eddies, as well as uncertainty about the forcing from the atmosphere (wind stress, heat and water exchange). A pioneering work with a realistic configuration of ocean basins was carried out by Takano, Mintz and Han (unpublished, 1973) and reviewed by Takano (1979). In that study, density was a function of temperature only, so that the transport of heat there corresponded to transports of heat and salt in the real ocean. Meehl et al. (1982) used the coefficient of horizontal diffusion of heat of 2×10^4 m^2 s^{-1} for the experiment DOC1, while the value was changed to 1/10 of that for DOC2. The effect of the diffusion coefficient was large in the southern hemisphere as shown in the figure. In the northern hemisphere, the total value happened to be similar, even though the dominant component in DOC2 was the meridional overturning instead of diffusion as in DOC1. The result of a coupled ocean-atmosphere model by Manabe et al. (1979) is also shown. (The curve of energy transport is provided by Manabe, personal communication (1983)). The oceanic part of the model was the same as the oceanic model of Bryan and Lewis (1979), resulting in a similar small value of transport.

Miller et al. (1983) used the surface heat fluxes simulated by an atmospheric model with specified seasonally varying sea surface temperature, instead of observed surface fluxes, to evaluate the annual oceanic heat transport. Russell et al. (1985) extended the analysis to its seasonal variation. Their curve, included in Fig. 14(d), shows more resemblance to the FGGE ECMWF curve than to those calculated from surface heat budget studies. This perhaps supports the conjecture that a source of error in the surface heat budget method can be found in empirical formulae of radiation, since radiation at the surface is computed explicitly in models. It seems, however, that the resolution of their atmospheric model (8° latitude × 10° longitude) is insufficient for resolving heat transport by synoptic scale systems.

5. Concluding remarks

Figure 15 summarizes the annual mean transport by the atmosphere and the ocean evaluated in this study. In panel (a), ECMWF data are used, while in panel (b), GFDL data are used. In both cases, NFOV data of Nimbus 7 ERB experiment are used as the source of radiation information. Panel (c) shows the result of Carissimo et al. (1985) for comparison. Among two FGGE data sets, ECMWF data seem to give a better result here because of the smaller error of mass conservation and the better acceptance of southern hemisphere surface pressure observations.

The total transport by the atmosphere-ocean system is symmetric about the equator. This shape of the curve can be explained with a simple diffusion-type transport model (Stone, 1978). However, the contribution of either the atmosphere or the ocean is not similar between the two hemispheres. In particular, the ocean at 20–30°N carries more heat polewards than that of the same latitudes in the southern hemisphere, despite the oceanic area being smaller. To

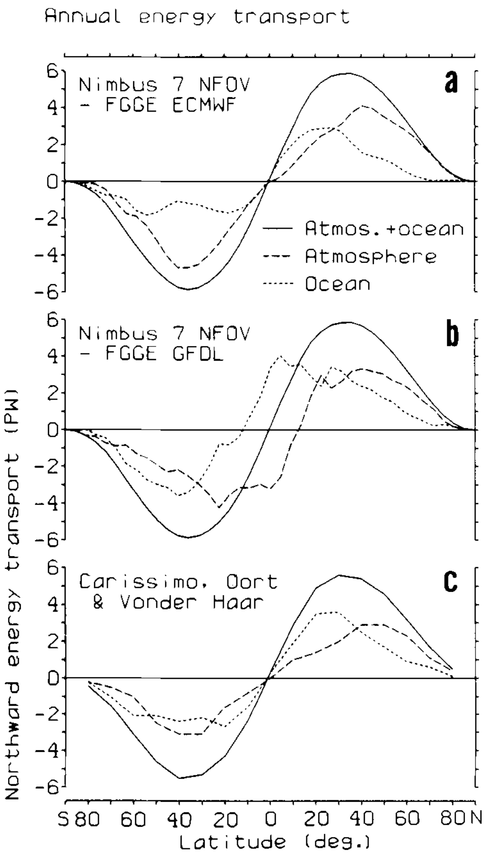

Fig. 15. The partition of annual mean northward transport of energy (solid lines) into the contribution of the atmosphere (dashed lines) and the ocean (dotted lines) evaluated with (a) Nimbus 7 NFOV and FGGE ECMWF data sets, (b) Nimbus 7 NFOV and FGGE GFDL data sets, and (c) by Carissimo et al. (1985).

explain the larger relative role of the ocean in the northern hemisphere, the following two mechanisms might be suggested. However, in contrast to the above observation, both are likely to have the largest contribution at 40–50° latitudes. (1) In the northern hemisphere, the eastern boundaries of the mid-latitude ocean enable the poleward geostrophic flow just below the Ekman layer to counter-balance the equator-ward Ekman transport under a westerly wind. The result is a larger poleward heat transport by the ocean in the northern hemisphere than the southern hemisphere (Bryan and Lewis, 1979). (2) In the nothern hemisphere, there is a larger area of land that has less heat capacity than the sea, so the thermal gradient between the tropics and the polar latitudes is smaller in summer, resulting in smaller heat transport by the atmosphere.

A difference of 2 PW was found in the oceanic heat transport of the northern subtropics between the residual estimate by Carissimo et al. (1985) and the estimate from surface heat balance by Hsiung (1985). If the result of the present study with ECMWF data is chosen as representative of the residual method, the unexplained discrepancy is reduced to 1 PW. The difference between the results of this study and Carissimo et al.'s mainly comes from the atmospheric transport, in particular, from the larger poleward heat and moisture transports by transient eddies in middle latitudes.

Significant advances of data assimilation technology came out after the production of the "main IIIb" data sets. Both ECMWF and GFDL made so-called "final IIIb" data sets with revised schemes and the revised FGGE database (Kållberg and Uppala, 1985; Stern and Ploshay, 1987). ECMWF has introduced diabatic heating in the initialization process. GFDL has revised the assimilation scheme to reduce gravity-wave noise and to achieve better acceptance of isolated observations. In addition, GFDL now archives assimilated fields on sigma levels, and ECMWF has adopted the interpolation of difference from the initial guess in the conversion from sigma to pressure coordinates. Both are likely to reduce the error in the conservation of mass. The period of the new assimilation is limited to the Special Observing Periods of FGGE (January-February and May-June), however. If data of the whole year could be assimilated with the currently best schemes, the overall accuracy would be considerably better than the results with the "main IIIb", though assimilation of the divergent wind and moisture is still in its developing stage.

The representativeness of the FGGE year is another problem. It will be necessary to use data of several years after FGGE to evaluate interannual variability of energy transport.

6. Acknowledgements

I am indebted to numerous persons including those who planned and conducted FGGE and ERB experiments. In particular, I am grateful to

Masao Kanamitsu, Masaru Chiba, Isao Kubota, Koji Yamazaki, Akimasa Sumi, Nobuo Sato and Tatsuya Iwashima for making FGGE data available to this study, to Ngar-Cheung Lau for arranging the GFDL FGGE statistics tape, to the Nimbus 7 ERB Experiment team (Head: H. Jacobowitz) and World Data Center A for Rockets and Satellites for providing the Nimbus 7 MATRIX data, to R. A. Schiffer, I. Kubota and Isamu Yagai for providing a preliminary version of MATRIX data, to M. Kanamitsu, Kikuro Miyakoda and Jeffrey Ploshay for sending orography data of ECMWF and GFDL models. I thank Taroh Matsuno, Syukuro Manabe and Tomio Asai for the initial suggestion of this subject and continuous encouragements. Computation is performed with the HITAC M280H computer at the Computer Centre, University of Tokyo (CCUT). The subroutine HWSSSP developed by John Adams, Paul Swarztrauber and Roland Sweet at the National Center for Atmospheric Research (NCAR), USA, is used to solve Poisson's equation on a sphere. Graphics subroutines of NCAR, adapted to CCUT environment, are also used.

REFERENCES

Arking, A. and Vemury, S. 1984. The NIMBUS 7 ERB data set: A critical analysis. *J. Geophys. Res. 89*, 5089–5097.

Bengtsson, L. 1983. The ECMWF level III-b data set. *GWE Newsletter No. 1*, 1–7 [Washington D.C.: U.S. Committee for GARP, National Academy of Sciences].

Bengtsson, L., Kanamitsu, M., Kållberg, P. and Uppala, S. 1982. FGGE 4-dimensional data assimilation at ECMWF. *Bull. Amer. Meteor. Soc. 63*, 29–43.

Bennett, A. F. 1978. Poleward heat fluxes in southern hemisphere oceans. *J. Phys. Oceanogr. 8*, 785–798.

Boer, G. J. 1986. A comparison of mass and energy budgets from two FGGE datasets and a GCM. *Mon. Wea. Rev. 114*, 885–902.

Boer, G. J. and Sargent, N. E. 1985. Vertically integrated budgets of mass and energy of the globe. *J. Atmos. Sci. 42*, 1592–1613.

Bourke, W., Seaman, R. and Puri, K. 1985. Data assimilation. *Adv. Geophys. 28B*, 123–155.

Bryan, K. 1982. Polward heat transport by the ocean: Observations and models. *Ann. Rev. Earth Planet. Sci. 10*, 15–30.

Bryan, K. and Lewis, L. J. 1979. A water mass model of the world oceans. *J. Geophys. Res. 84*, 2503–2517.

Budyko, M. I. 1971. *Climate and life*. Leningrad: Gidrometeoizdat. [English edition, 1974, New York: Academic Press, 508 pp.]

Campbell, G. G. and Vonder Haar, T. H. 1980. Climatology of radiation budget measurements from satellites. *Atmospheric Science Paper No. 323*, 74 pp. [Fort Collins, CO, USA: Colorado State University].

Carissimo, B. C., Oort, A. H. and Vonder Haar, T. H. 1985. Estimating the meridional energy transports in the atmosphere and the ocean. *J. Phys. Oceanogr. 15*, 82–91.

Daley, R. 1985. The analysis of synoptic scale divergence by a statistical interpolation procedure. *Mon. Wea. Rev. 113*, 1066–1079.

Guymer, L. B. and Le Marshall, J. F. 1980. Impact of FGGE bouy data on southern hemisphere analyses. *Australian Meteorological Magazine 28*, 19–42 [reproduced in *Bull. Amer. Meteor. Soc. 62*, 38–47].

Han, Y.-J. 1984. A numerical world ocean general circulation model, Part II: A baroclinic experiment. *Dyn. Atmos. Oceans, 8*, 141–172.

Hartmann, D. L., Ramanathan, V., Berroir, A. and Hunt, G. E. 1986. Earth radiation budget data and climate research. *Rev. Geophys. 24*, 439–468.

Hastenrath, S. 1980. Heat budget of tropical ocean and atmosphere. *J. Phys. Oceanogr. 10*, 159–170.

Hastenrath, S. 1982. On meridional heat transports in the world ocean. *J. Phys. Oceanogr. 12*, 922–927.

Hsiung, J. 1985. Estimates of global oceanic meridional heat transport. *J. Phys. Oceanogr. 15*, 1405–1413.

Ikawa, M. 1984: Generalization of multivariate optimum interpolation method and the roles of linear constraint and covariance matrix in the method. Part 1: in discrete form. *Papers in Meteorology and Geophysics 35*, 81–102 [Tsukuba, Japan: Metereological Research Institute].

Jacobowitz, H., Tighe, R. J. and the NIMBUS 7 ERB experiment team, 1984a. The earth radiation budget derived from the NIMBUS 7 ERB experiment. *J. Geophys. Res. 89*, 4997–5010.

Jacobowitz, H., Suole, H. V., Kyle, H. L., House, F. B. and the NIMBUS 7 ERB experiment team, 1984b. The Earth Radiation Budget (ERB) experiment: an overview. *J. Geophys. Res. 89*, 5021–5038.

Julian, P. R. 1983. Comments on the ECMWF IIIb analysis data set. *GWE Newsletter No. 1*, 15–17.

Julian, P. R. 1985. Some comparison of ECMWF IIIb and GFDL IIIb analyses in the tropics. *Proceeding of the 1st National Workshop on the Global Weather Experiment 2(1)*, 211–216. [Washington, D.C.: National Academy of Sciences].

Kållberg, P. and Uppala, S. 1985. Reprocessing of the final FGGE level II-b data at ECMWF. *GWE Newsletter No. 11*, 1–12.

Kung, E. C. and Tanaka, H. 1983. Energetics analysis of the global circulation during the special observation periods of FGGE. *J. Atmos. Sci. 40*, 2575–2592.

Lambert, S. J. 1983. List of known or suspected problems with the ECMWF analyses of FGGE data. *GWE Newsletter No. 1*, 25.

Lau, N.-C. 1984a. Circulation statistics based on FGGE level III-b analyses produced by GFDL. *NOAA Data Report ERL GFDL-5*, 427 pp. [Princeton: GFDL/NOAA].

Lau, N.-C. 1984b. A comparison of circulation statistics based on FGGE level III-b analyses produced by GFDL and ECMWF for the special observing periods. *NOAA Data Report ERL GFDL-6*, 237 pp.

Lau, N.-C. 1985. Publication of circulation statistics based on FGGE level III-b analyses produced by GFDL and ECMWF. *Bull. Amer. Meteor. Soc. 66*, 1293–1301.

Lorenc, A. 1981. A global three-dimensional multivariate statistical interpolation scheme. *Mon. Wea. Rev. 109*, 721–791.

Lorenc, A. and Tibaldi, S. 1980. The treatment of humidity in ECMWF's data assimilation scheme. In *Atmospheric water vapor* (ed. A. Deepak, T. D. Wilkerson and L. H. Ruhnke). New York: Academic Press, 497–511.

Manabe, S., Bryan, K. and Spelman, M. J. 1979. A global ocean-atmosphere climate model with seasonal variation for future studies of climate sensitivity. *Dyn. Atmos. Oceans, 3*, 393–426.

Masuda, K. 1988. Problem notes about FGGE "main" IIIb datasets of ECMWF and GFDL. *Tenki* (Bulletin of the Meteorological Society of Japan), *35*, 5–19 (in Japanese). English version is available from the author as *Meteorological Research Report 87-01*, Division of Meteorology, Geophysical Institute, University of Tokyo.

Meehl, G. A., Washington, W. M. and Semtner, A. J. Jr. 1982. Experiments with a global ocean model driven by observed atmospheric forcing. *J. Phys. Oceanogr. 12*, 301–312.

Miller, J. R., Russell, G. L. and Tsang, L.-C. 1983. Annual oceanic heat transport computed from an atmospheric model. *Dyn. Atmos. Oceans 7*, 95–129.

Miyakoda, K., Ploshay, J. and Stern, W. 1983. Guide and caution on the GFDL/FGGE data set. *GWE Newsletter No. 1*, 8–14.

Newton, C. W. 1972. Southern hemisphere general circulation in relation to global energy and momentum balance requirements. *Meteor. Monogr. no. 35*, 215–246.

Oort, A. H. 1983. Global atmospheric circulation statistics, 1958–1973. *NOAA Professional Paper No. 14*, 180 pp. + microfiches.

Oort, A. H. and Peixóto, J. P. 1983. Global angular momentum and energy balance requirements from observations. *Adv. Geophys. 25*, 355–490.

Oort, A. H. and Vonder Haar, T. H. 1976. On the observed annual cycle in the ocean-atmosphere heat balance over the northern hemisphere. *J. Phys. Oceanogr. 6*, 781–800.

Peixóto, J. P. and Oort, A. H. 1983. The atmospheric branch of the hydrological cycle and climate. In *Variations in the global water budget* (ed. A. Street-Perrot, M. Beran and R. Ratcliffe). Dordrecht: Reidel, 5–65.

Puri, K. and Stern, W. 1985. Investigations to reduce noise and improve data acceptance in the GFDL 4-dimensional analysis system. In *Seminar/Workshop 1984, Data assimilation systems and observing system experiments with particular emphasis on FGGE, Vol. 2*, 157–190 [Reading, U.K.: ECMWF].

Russell, G. L., Miller, J. R. and Tsang, L.-C. 1985. Seasonal oceanic heat transports computed from an atmospheric model. *Dyn. Atmos. Oceans 9*, 257–271.

Stern, W. F. and Ploshay, J. J. 1987. The post-FGGE data assimilation system at GFDL. *GWE Newsletter No. 17*, 5–13.

Stern, W. F., Ploshay, J. J. and Miyakoda, K. 1985. Continuous data assimilation at GFDL during FGGE. In *Seminar/Workshop 1984, Data assimilation systems and observing system experiments with particular emphasis on FGGE, Vol. 2*, 125–156 [Reading, U.K.: ECMWF].

Stone, P. H. 1978. Constraints on dynamical transports of energy on a spherical planet. *Dyn. Atmos. Oceans 2*, 123–139.

Sverdrup, H. U. 1957. Oceanography. In *Handbuch der Physik 48*, 630–638 [Berlin: Springer].

Takano, K. 1979. Comments on global models of the oceanic general circulation. *Dyn. Atmos. Oceans 3*, 339–343.

Talley, L. D. 1984. Meridional heat transport in the Pacific Ocean. *J. Phys. Oceanogr. 14*, 231–241.

Trenberth, K. E. 1979. Mean annual poleward energy transports by the oceans in the southern hemisphere. *Dyn. Atmos. Oceans 4*, 57–64.

Trenberth, K. E. 1984. Interannual variability of the southern hemisphere circulation: Representativeness of the year of Global Weather Experiment. *Mon. Wea. Rev. 112*, 108–123.

Vonder Haar, T. H. and Oort, A. H. 1973. New estimate of annual poleward energy transport by northern hemisphere oceans. *J. Phys. Oceanogr. 3*, 169–172.